BMC Cell Biology

Research article

The new anti-actin agent dihydrohalichondramide reveals fenestrae-forming centers in hepatic endothelial cells

Filip Braet*[1], Ilan Spector[2], Nava Shochet[2], Phillip Crews[3], Tatsuo Higa[4], Eline Menu[5], Ronald de Zanger[1] and Eddie Wisse[1]

Address: [1]Laboratory for Cell Biology and Histology, Free University of Brussels (VUB), Laarbeeklaan 103, 1090 Brussels-Jette, Belgium, [2]Department of Physiology and Biophysics, Health Science Center, State University of New York at Stony Brook (SUNY), Stony Brook, NY 11794-8661, New York, USA, [3]Department of Chemistry and Biochemistry, University of California, Santa Cruz, CA 9506, USA, [4]Department of Marine Sciences, University of the Ryukyus, Nishihara, Okinawa 903-01, Japan and [5]Department of Hematology and Immunology, Free University of Brussels (VUB), Laarbeeklaan 103, 1090 Brussels-Jette, Belgium

E-mail: Filip Braet* - filipbra@cyto.vub.ac.be; Ilan Spector - ispector@epo.som.sunysb.edu; Nava Shochet - nshochet@epo.som.sunysb.edu; Phillip Crews - crews@chemistry.ucsc.edu; Tatsuo Higa - thiga@sci.u-ryukyu.ac.jp; Eline Menu - Eline.Menu@vub.ac.be; Ronald de Zanger - ronald@cyto.vub.ac.be; Eddie Wisse - wisse@cyto.vub.ac.be

*Corresponding author

Abstract

Background: Liver sinusoidal endothelial cells (LSECs) react to different anti-actin agents by increasing their number of fenestrae. A new structure related to fenestrae formation could be observed when LSECs were treated with misakinolide. In this study, we investigated the effects of two new actin-binding agents on fenestrae dynamics. High-resolution microscopy, including immunocytochemistry and a combination of fluorescence- and scanning electron microscopy was applied.

Results: Halichondramide and dihydrohalichondramide disrupt microfilaments within 10 minutes and double the number of fenestrae in 30 minutes. Dihydrohalichondramide induces fenestrae-forming centers, whereas halichondramide only revealed fenestrae-forming centers without attached rows of fenestrae with increasing diameter. Correlative microscopy showed the absence of actin filaments (F-actin) in sieve plates and fenestrae-forming centers. Comparable experiments on umbilical vein endothelial cells and bone marrow sinusoidal endothelial cells revealed cell contraction without the appearance of fenestrae or fenestrae-forming centers.

Conclusion: (I) A comparison of all anti-actin agents tested so far, revealed that the only activity that misakinolide and dihydrohalichondramide have in common is their barbed end capping activity; (II) this activity seems to slow down the process of fenestrae formation to such extent that it becomes possible to resolve fenestrae-forming centers; (III) fenestrae formation resulting from microfilament disruption is probably unique to LSECs.

Background

Liver sinusoidal endothelial cells (LSECs) differ from other endothelial cells. They possess open fenestrae that are grouped in sieve plates and lack a basal lamina [1]. Fenestrae measure about 150 nm and occupy 6–8% of the endothelial surface (porosity) [2,3]. The endothelial filter

characteristics determine the exchange between the blood and the hepatocytes, and are affecting the hepatic metabolism of lipoproteins including cholesterol and vitamin A [4]. Structural integrity of the fenestrated sinusoidal liver endothelium is believed to be essential for the maintenance of a normal exchange of fluids, solutes, particles and metabolites between the sinusoidal blood and hepatocytes. In the past, numerous publications appeared about the role of these dynamic structures under various physiological and pathological situations [5]. Their role and involvement in the regenerating liver after partial hepatectomy [6], shear stress [7], liposome-mediated transport [8], liver cancer [9], injury by free radicals [10] and chronic alcohol abuse [11], resulting in alcoholism-associated hyperlipoproteinemia [12] have been explored.

In response to external signals, dynamic changes in fenestrae diameter and number occur and involve the dynamics of the actin cytoskeleton [13]. Discoveries in the past decade have revealed that an actomyosin-driven machinery contributes to the regulation of fenestrae diameter and this under the control of intracellular calcium levels [14–16]. Detergent-extracted whole mounts of LSECs showed that fenestrae are delineated by a fenestrae-associated cytoskeleton ring (FACR), which changes in diameter and thickness after different treatments. These rings therefore seem to act as a supporting lattice and "muscle" around fenestrae [17]. Furthermore, the actin cytoskeleton of LSECs has been shown to participate in cellular processes such as chemical- and cold-induced cell injury during liver transplantation [18,19].

The recent availability of a battery of new actin binding drugs that affect the polymerization of actin by different mechanisms, provide a powerful tool to dissect the dynamics and functions of the actin cytoskeleton in various cell types [20]. Previously it has been demonstrated that the treatment of LSECs with cytochalasin B [21], latrunculin A [22], swinholide A, misakinolide or jasplakinolide [23], induce an increase in the number of fenestrae. Only after treating LSECs with misakinolide, it was possible to resolve the process of fenestrae formation and to identify a new structure involved in the process of fenestrae formation [23]. This illustrates the importance of the use of different anti-actin drugs to study the dynamic cellular processes that depend on the integrity and function of actin.

The present study endeavours to elucidate the dynamic process of *de novo* formation of LSEC fenestrae by correlating specific changes in actin organization with fenestrae. We used two novel actin-binding compounds derived from marine organisms, halichondramide (HALI) and di-hydrohalichondramide (di-h-HALI), that belong to a large group of structurally related marine macrolides [20]. Experiments on various cell lines show that HALI induces almost complete depletion of F-actin within minutes, illustrating the F-actin severing and monomer sequestering activities. Di-h-HALI, which differs from HALI only in having a single bond in the macrolide at positions 4–5 instead of a double bond, altered the filamentous F-actin distribution into large F-actin aggregates, and was found to possess strong barbed-end capping and weak severing activities [20]. Both agents possess biochemical similarities to the previous tested anti-actin drugs swinholide and misakinolide which have severing and barbed-end capping activities, respectively [20,23].

We report here that HALI and di-h-HALI: (I) disrupts actin organization in LSECs in a distinctive manner; (II) significantly increase the number of fenestrae; (III) that di-h-HALI elicits fenestrae-forming centers (FFCs) from which nascent fenestrae are fanning out; and (IV) for reasons of comparison, we also examined the effect of HALI and di-h-HALI on cultured human umbilical vein endothelial cells (HUVECs) and bone marrow sinusoidal endothelial cells (BECs STR-4). It was reported earlier that various treatments could induce fenestrae in HUVECs [24,25]; whereas sinusoidal endothelial cells derived from the bone marrow posses the capacity to form transendothelial openings in vivo (i.e., transendothelial channels and diaphragmed fenestrae) while these structures are lost or greatly reduced in number in vitro [26,27]. Therefore, the effect of HALI and di-h-HALI on BECs STR-4 was investigated to address the question whether these microfilament-disrupting drugs could induce fenestrae in this cell line derived from another sinusoidal source.

Results
Fluorescence microscopy
In untreated LSECs, rhodamine-phalloidin staining reveals intense circular bundles lining the cell periphery and straight bundles traversing the cytoplasm. Whereas G-actin staining was most intense at the perinuclear region, and diffusely distributed in the cytoplasm (Fig. 1A). Exposure of cells to 100 nM HALI or di-h-HALI resulted in a loss of actin bundles and in the appearance of a drug-specific F-, and G-actin pattern (Fig. 1B, 1C). Maximal effects of HALI and di-h-HALI were obtained after 10 minutes treatment, and further incubation did not result in additional alteration of actin organization. With HALI, F-actin staining disappeared almost completely and only a weak speckled fluorescence could be observed in the entire cytoplasm, with only a few short and fine fibers remaining mainly at the cell margin. The rapid and massive F-actin depolymerization was reflected in a significant increase in G-actin, which was diffusely distributed in the cytoplasm (Fig. 1B). Di-h-HALI treatment caused complete dissolution of cytoplasmic F-actin bundles and appearance of nu-
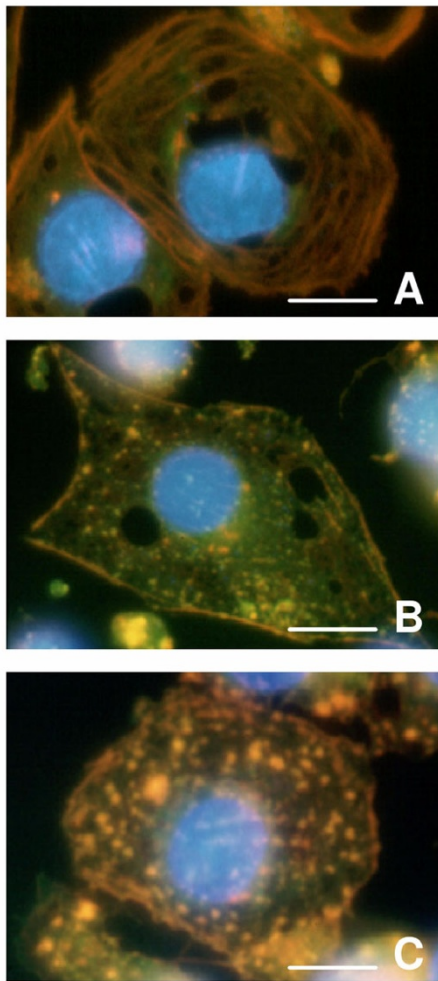
Figure I
Fluorescence micrographs showing the effects of HALI and di-h-HALI on actin organization in LSECs, monitored with rhodamine-phalloidin (F-actin / red) and fluorescein-DNase I staining (G-actin / green). Blue color represents the nucleus stained with DAPI. (**A**) F-actin distribution in control LSECs shows the presence of cytoplasmic stress fibers and peripheral bands of actin bundles that line the cell margin. Note that G-actin is mainly localized in the perinuclear region. (**B**) LSECs treated with 100 nM HALI for 10 minutes, show a loss of cytoplasmic F-actin bundles and peripheral F-actin bands are less dense, whereas the cytoplasm is faintly stained and only few small F-actin dots and short fine filaments remaining. G-actin fluorescence increased markedly as compared to control LSECs and is distributed thorough the cytoplasm. (**C**) LSECs treated with 100 nM of di-h-HALI for 10 minutes show loss of F-actin bundles and appearance of brightly stained F-actin patches. Peripheral F-actin bands are still present, and furthermore G-actin is diffuse and faintly stained as compared to HALI-treated LSECs. Scale bars, 5 μm.

merous bright F-actin patches in the cytoplasm, whereas the peripheral F-actin bundles showed interruptions and became less dense. Furthermore, G-actin staining was not increased in intensity and was mainly localized around the nuclear area as in untreated cells (Fig. 1C).

Lower concentrations of both compounds (25 and 50 nM) resulted in partial loss of F-actin bundles that were present even after 120 minutes incubation. Exposure to higher concentrations of HALI or di-h-HALI (200 nM) resulted in a decreased viability as assessed by the percentage of cells stained by propidium iodide: from 97% (control) to 59% and 65% respectively.

Scanning electron microscopy
To examine the effects of the two actin-binding agents on LSEC fenestration, purified cells were grown on collagen-coated cover slips and prepared for SEM. In these experiments, we treated cells with 100 nM of one of the compounds, because at this concentration the actin cytoskeleton was disassembled without further adverse effects on cell shape and viability. Untreated LSECs showed good preservation of their surface ultrastructural characteristics (Fig. 2A), revealing a central, bulging nucleus, surrounded by flat cytoplasmic extensions that contained fenestrae clustered in sieve plates. Within 30–60 minutes of di-h-HALI treatment, small cytoplasmic unfenestrated areas, surrounded by rows of very small fenestrae appeared, suggesting nascent fenestrae emerging from those areas (Fig. 2B). Curiously, HALI-treated LSECs did show such unfenestrated areas, and rows of very small fenestrae were absent even with different exposure times and concentrations. Because SEM gathers surface information with limited resolution, we prepared whole-mounts, and ultrathin sections for TEM to examine these peculiar areas in fine detail (vide infra).

While the maximum effect of the two drugs on actin organization was reached after 10 minutes, the maximum effect of the drugs on the number of fenestrae was reached at 120 minutes. Figure 2C depicts a di-h-HALI-treated LSEC after 120 minutes exposure to 100 nM di-h-HALI. The same SEM morphology was also seen in HALI-treated cells. Fenestrae were no longer clustered in sieve plates embedded in unfenestrated areas of cytoplasm (Fig. 2A), but treated cells contained abundant numbers of fenestrae interchanged with long and thin cytoplasmic arms, extending from the nucleus (Fig. 2C). Inside the fenestrated cytoplasm, the presence of small cytoplasmic unfenestrated areas could be observed. However, these areas were devoid of rows of very small fenestrae.

Computer-assisted analysis of endothelial fenestration, using digitized SEM images, showed that fenestrae occur at a frequency of 3.0 ± 0.2 per micrometer squared in con-
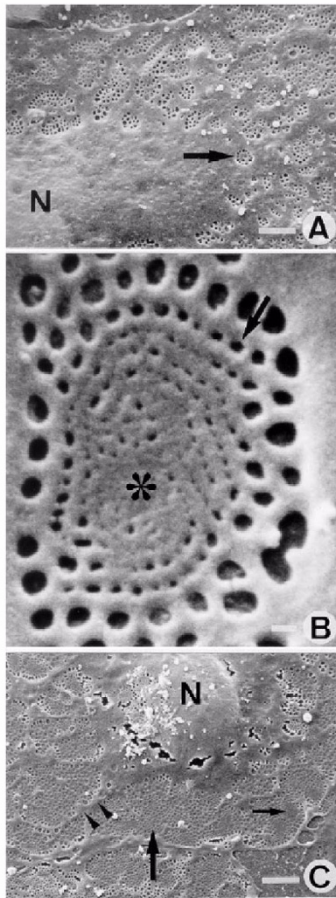
Figure 2
Scanning electron microscopic (SEM) observations showing the surface topology of control-, and di-h-HALI-treated LSEC. (**A**) SEM micrograph of a control LSEC shows the presence of numerous fenestrae grouped in sieve plates (arrow). The bulging area contains the nucleus (N). Scale bar, 2 μm. (**B**) High-power SEM micrograph of the fenestrated cytoplasm obtained after 60 minutes exposure to 100 nM di-h-HALI. Note a typical cytoplasmic unfenestrated area (asterisk), surrounded by circular rows of very small fenestrae (arrow), suggesting nascent fenestrae fanning out into the surrounding fenestrated cytoplasm. Scale bar, 250 nm. (**C**) Shows a SEM micrograph of a LSEC treated with 100 nM di-h-HALI for 120 minutes, revealing a substantially increased number of fenestrae (large arrow). Thin nonfenestrated cytoplasmic arms (arrowheads) divide the cytoplasm into large sieve plates. In the fenestrated cytoplasm, small cytoplasmic unfenestrated areas devoid of connected fenestrae rows could be observed (small arrow), nucleus (N). Scale bar, 2 μm.

Figure 3
Effect of HALI and di-h-HALI on the number of fenestrae per micrometer squared in time. From this graph, we can conclude that both agents increase the number of fenestrae, although at a different rate and different maximum. Data are means plus or minus S.E.M. of triplicate determinations. Note the significant differences between control LSECs (0 minutes) and treated LSECs, as indicated by asterisks (p < 0.01) or by triangles (p < 0.05) (Mann-Whitney U test, two-sided). No significant difference in the number of fenestrae was observed at the 0.05 confidence level between 60 and 120 minutes of treatment with HALI or di-h-HALI.

trol LSEC. By comparing the effects of both microfilament-disrupting agents (at 100 nM) as a function of time, it becomes clear that HALI increases the number of fenestrae faster than di-h-HALI (Fig. 3). A significant difference in the number of fenestrae between control and
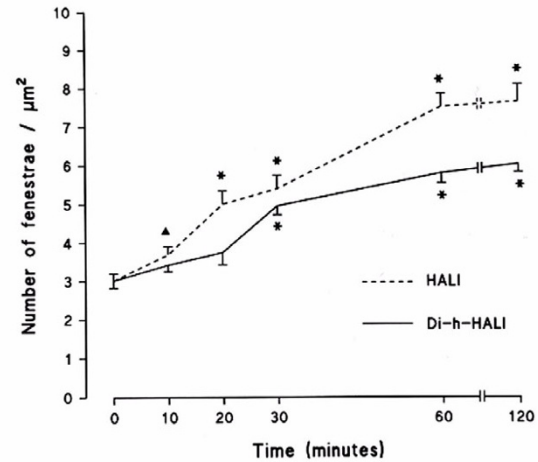
HALI-treated LSECs could be discerned as early as 10 minutes after HALI application. In the case of di-h-HALI, a significant difference in the number of fenestrae was observed 20 minutes later than HALI (Fig. 3), corresponding with the observation of FFCs with connected fenestrae rows (Fig. 2B). After 120 minutes in the presence of HALI or di-h-HALI, the number of fenestrae per micrometer squared increased to 7.7 ± 0.5, and 6.0 ± 0.2 respectively. Lowering the concentrations of HALI or di-h-HALI to 25 or 50 nM gave insignificant changes in the number of fenestrae (data not shown).

We also measured the effect of the agents on fenestrae diameter at the end of treatment (Table 1 and Fig. 4). Fenestrae of HALI- or Di-h-HALI-treated LSECs have a mean diameter of 182 ± 75 nm and 165 ± 60 nm, respectively. A significant difference was found between the control and HALI- or Di-h-HALI-treated LSECs at the 0.0001 confidence level (Table 1, Fig. 4).

To address the question whether actin-disruption could induce fenestrae and reveal FFCs in large vessel and other capillary endothelial cells as well, the effect of 25, 50, 100
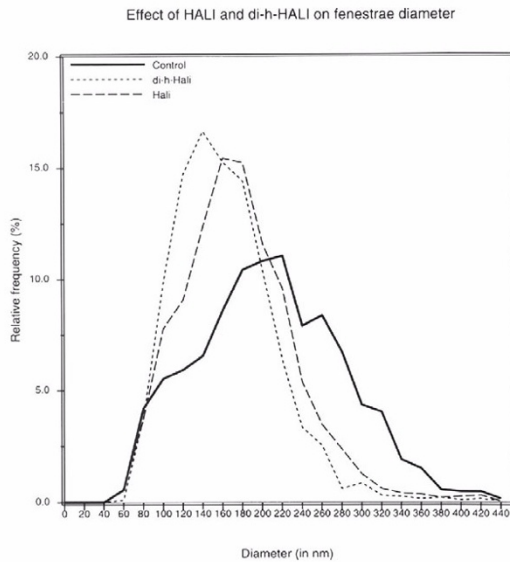
Figure 4
Diameter distribution of fenestrae, showing values for control, HALI, and di-h-HALI – treated LSECs, extending the data of fenestrae diameter of Table1. From this graph, we can conclude that treatment of LSECs with HALI or di-h-HALI results in smaller fenestrae diameters.

Table 1: Fenestrae diameter (nm) after treatment with HALI or di-h-HALI obtained by scanning electron microscopy

	Fenestrae diameter (nm)	± S.D.	± S.E.M.
Control	212	82	2.3
HALI	182*	75	1.7
di-h-HALI	165*	60	1.3

Note. Comparison of fenestrae diameter between control, HALI- and di-h-HALI-treated LSECs. Results are expressed as mean ± standard deviation (S.D.) and ± standard error of the mean (S.E.M). Data are obtained from three different experiments. * Significant difference in diameter of fenestrae between the control and the LSECs treated with HALI (100 nM for 2 hours) and di-h-HALI (100 nM for 2 hours), ($p < 0.0001$; Mann-Whitney U test – two sided).

Figure 5
SEM observations of HUVECs (A-B) and BECs STR-4 (C-D) treated with 100 nM di-h-HALI for 120 min. (A) HUVECs exposed to di-h-HALI show significant signs of cell contraction; i.e. the cytoplasm is retracted and numerous fine cytoplasmic extensions appear (arrows). Scale bar, 5 μm. **(B)** High magnification image of the cytoplasm shows a smooth surface and the lack of fenestrated structures (compare with Fig. 2C for the difference with LSECs). Scale bar, 2.5 μm. **(C-D)** di-h-HALI treated BECs STR-4 show features similar to those seen in A and B (scale bars [C] 5 μm, [D] 2.5 μm).

and 200 nM HALI or di-h-HALI for 10, 20, 30, 60 and 120 minutes was examined on cultured HUVECs and BECs STR-4 (Fig. 5). At all concentrations and incubation times, both cell types changed their morphology from well-spread to a more retracted appearance, but they never rounded up completely (Fig. 5A, 5C). Rhodamine-phalloidin stain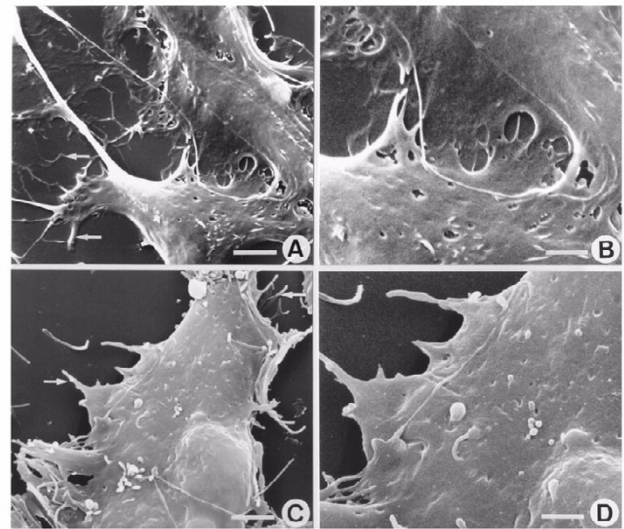ing revealed a complete F-actin dissolution as early as 30 minutes after treatment for both anti-actin agents when concentrations higher than 50 nM were used (data not shown). Detailed investigation of the topology of Di-h-HALI-treated HUVECs (Fig. 5B) and BECs STR-4 (Fig. 5D) revealed no sign of fenestrae and connected fenestrae rows, instead smooth cytoplasmic processes surrounding the bulging nucleus could be observed.

Correlative fluorescence- and scanning electron microscopy

Fenestrae in vitro have a diameter in the order of 200 nm (Table 1), making it necessary to use electron microscopy for their study (Fig. 2). Therefore, to correlate fluorescently-labeled actin structures with SEM information, we combined one fluorescent and one SEM image of the same cell. This enables us to correlate actin and fenestrae-forming center topology. Examination of control LSECs stained for F-actin (Fig. 6A) and subsequently prepared for SEM (Fig. 6B), revealed features as shown in Fig. 1A and Fig. 2A, respectively. Projecting the green colored SEM micrograph on top of the corresponding red rhodamine-phalloidin stained LSEC, clearly illustrates a structural relation between F-actin and the surface topology of the cell

(Fig. 6C). Dense peripheral actin filaments lined the cell margins, while straight actin fibers are mainly running in the peripheral cytoplasm. Close examination revealed negligible staining for F-actin in the nuclear area. Furthermore, F-actin was absent inside the fenestrated areas. However, actin filaments were running closely alongside the sieve plates (Fig. 6C). After 10 min of di-h-HALI treatment, the F-actin filaments are disrupted (Fig. 6D), sieve plates are clearly visible (Fig. 6E) and no sign of F-actin could be found inside these fenestrated areas (Fig. 6F). Moreover, the images show that the brightly stained F-actin patches as observed in Fig. 1C match with the fine globular topographic elevations present on the thin non-fenestrated arms which divide the cytoplasm in sieve plates (Fig. 6D, 6E, 6F). Thorough investigation of LSECs treated with di-h-HALI for 60 min, provided evidence that FFCs and the surrounding area are devoid of F-actin (Fig. 6G, 6H, 6I). Figure 6J illustrates that prolonged exposure to 100 nM di-h-HALI for 120 min did not result in additional alterations in actin organization (see also, Fig. 1C). At this time, the maximum effect of di-h-HALI on the fenestral number was reached (Fig. 6K), resulting in huge sieve plates which are lacking any sign of F-actin staining (Fig. 6L).

Transmission electron microscopy
One of the most straightforward ways to observe the complex architecture of the cytoskeleton is to examine whole mounts of cells by TEM [28]. This technique, allows the visualization of the cytoskeleton at the supramolecular level with a minimal disruption to the cells. Examination of control LSECs at low magnification showed the presence of an extensive network of cytoskeletal elements that fills the cytoplasm adjacent to the sieve plates (Fig. 7A). LSEC fenestration is characterized by the presence of a sieve plate-, and a fenestrae-associated cytoskeleton connected to a framework of microtubules and microfilaments [17]. Treatment with 100 nM HALI or di-h-HALI for 10 to 20 minutes resulted in the disappearance of microfilaments, and in the appearance of small cytoplasmic unfenestrated areas of intermediate electron density (gray centers), localized around the nucleus of all treated LSECs was apparent (Fig. 7B). Remarkably, between 30–60 minutes of di-h-HALI treatment, FFCs could be observed in all of these cells, consisting of rows of fenestrae, fanning out into the surrounding cytoplasm (Fig. 7C, 7D). Examination at higher magnification, reveals that these rows of fenestrae are clearly connected to the gray centers and that fenestrae with increasing diameter are emanating in the surrounding fenestrated cytoplasm (Fig. 7D). These structures are suggestive of de novo fenestrae formation and are similar to the recently described FFCs as revealed with the actin inhibitor misakinolide [23]. Even in static EM images these spiraling rows of fenestrae give the impression of a dynamic process, in which the newly formed fe-

nestrae ebb away in the surrounding fenestrated cytoplasm as a tornado. This assumption was confirmed by quantifying the number of fenestrae rows connected to one FFC after different times of di-h-HALI treatment (Fig. 8), revealing that the onset of fenestrae formation starts after 10 min treatment and reaches its maximum after 60 min di-h-HALI treatment. At 120 min of treatment, when the burst of fenestrae formation has subsided (Fig. 7E), a significant shift towards a negligible low number of connected fenestrae rows could be registered (Fig. 8). At this time point, when the effect of di-h-HALI on the number of fenestrae reaches its maximum (Fig. 3), long cytoplasmic arms are extending from the nucleus into the cytoplasm and appear to divide the fenestrated cytoplasm into large sieve plates (Fig. 7E). At this stage, the burst of fenestrae formation has subsided and all fenestrae, including the newly formed ones, were delineated by the previously described FACR (Fig. 7F) with the same structure as in control LSECs [17]. Detailed and thorough investigation of HALI-treated LSECs at different times and concentrations only revealed the small unfenestrated areas (gray centers) that presumably represent inactive FFCs, but no sign of connected fenestrae rows.

In addition to the whole-mount TEM method, ultrathin sectioning was applied to cultured LSECs after treatment with 100 nM di-h-HALI at different time points. Examination of tangentially cut control LSECs shows two organizations of fenestrae as described previously [1,29]; i.e., a somewhat complex sponge-like appearance around the nucleus (Fig. 9A), and grouped fenestrae in the peripheral cytoplasm (Fig. 9B). Within 30–60 minutes of di-h-HALI treatment, FFCs could be observed within the peripheral cytoplasm. Sectioned FFCs (Fig. 9C) are comparable to those seen with the whole-mount TEM method (Fig. 7C). Despite complete microfilament-disruption (Fig. 1C), the cytoplasm surrounding the FFCs show a few thin electron dense filaments fanning out in the surrounding cytoplasm (Fig. 9C). After 120 minutes of treatment, FFCs could be observed within the sieve plates, and they did not show connected rows of fenestrae at this stage. Moreover, on the edges of the sieve plates some short and thin filaments could be observed. At high magnification, the FFCs show a fine granular pattern of intermediate electron density (Fig. 9D).

Transversely cut sections revealed no additional structural information (data not shown).

Discussion
Disassembly of filamentous actin in LSECs with the new microfilament-disrupting drug di-h-HALI enabled us to visualize FFCs (Figs. 2, 7, 9), most probably involved in the process of fenestrae formation, as demonstrated recently with the actin inhibitor misakinolide [20,23]. Ex-
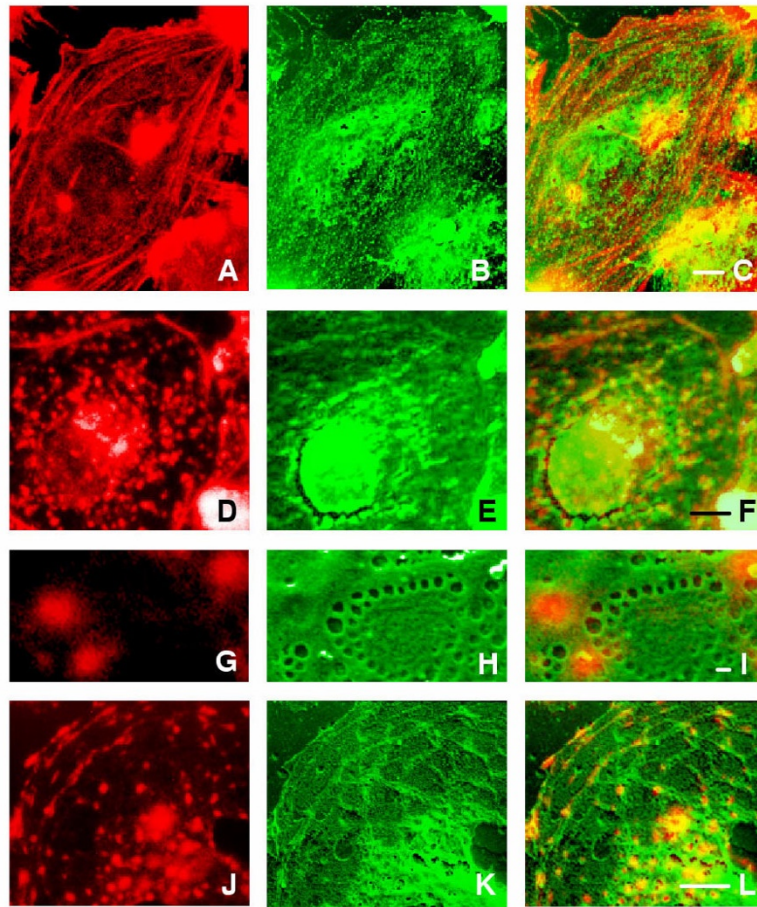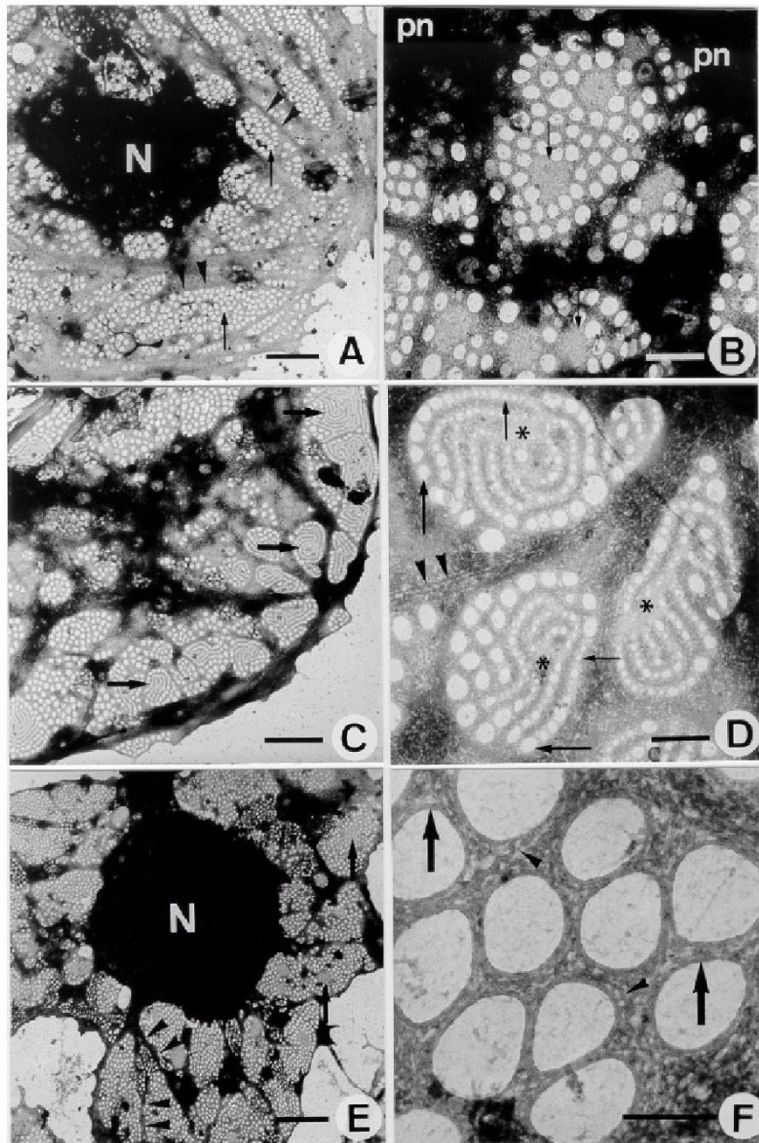
Figure 6
Correlative fluorescence-, and SEM micrographs of control (A-C) and microfilament-disrupted LSECs obtained after 10 min (D-F), 60 min (G-I) and 120 min (J-L) di-h-HALI treatment. Figure set shows simultaneous localization of fluorescent labeled F-actin (red) (left column) in combination with topographic SEM information (green) (middle column) and the merged image (right column) of the same cell. Control LSECs show features similar as those seen in Figs. 1A and 2A: i.e., a well developed filamentous actin cytoskeleton (**A**) and sieve plates (**B**). The merge image (**C**) reveals that the fenestrated areas are clearly interspersed between the actin filaments. Scale bar, 2 μm. After 10 min di-h-HALI treatment (**D-F**), the images show that the brightly stained F-actin dots matches with the fine globular topographic elevations present on the thin nonfenestrated cytoplasmic arms. Within one hour of di-h-HALI treatment (**G-I**), the merge image of the fenestrated area reveals that the FFC and the area around is devoid of F-actin. Scale bar, 200 nm. (**J-L**) Images obtained after 120 min of di-h-HALI treatment. Note that the F-actin dots are localized in the thin nonfenestrated cytoplasmic arms; while the highly fenestrated cytoplasm lacks F-actin. Scale bar, 2 μm.

posure of LSECs by other actin-perturbing agents including cytochalasin B [21], latrunculin A [22], swinholide A, jasplakinolide [23], and HALI (this paper) also produces a rapid increase in the number of fenestrae and the appearance of small unfenestrated areas which apparently represent inactive FFCs [23], indicating that actin disruption per se is sufficient to induce an increase in the number of fenestrae. However, the fact that only misakinolide and di-h-HALI resolved FFCs in the process of fenestrae formation indicate that specific alterations of the actin system are necessary to unmask active FFCs. Moreover, if our previous observations on FFCs as revealed by using misakinolide was an artefact of the drug, then it is most unlikely that di-h-HALI has the same side effect. The biochemical property that misakinolide and di-h-HALI have in common is their barbed end capping activity [20,30], however misakinolide also forms actin dimers, whereas di-h-HALI possesses weak F-actin severing activity. In both cases an increased number of fenestrae (Fig. 3) and FFCs (Fig. 2, 7, 9) [23] could be observed, but misakinolide increases the number of fenestrae more rapidly than di-h-HALI (Fig. 3) [23], while di-h-HALI revealed ap-

Figure 7
TEM micrographs of whole mount, formaldehyde prefixed, cytoskeleton buffer-extracted control LSEC (A), and di-h-HALI treated LSECs (B-F). (**A**) Low magnification showing the area containing the nucleus (N) and extracted cytoplasm. Note that the sieve plates are well defined by a dark border (arrowheads). Inside the sieve plates, fenestrae can be observed (small arrows). Scale bar, 2 μm. (**B**) Treatment with di-h-HALI for 10 to 20 minutes resulted in the appearance of small cytoplasmic unfenestrated areas of intermediate density (small arrows) lying in the neighbourhood of the perinuclear area (pn). Scale bar, 1 μm. (**C**) Within 30–60 minutes of treatment, small cytoplasmic unfenestrated areas of intermediate density (arrows) could be observed within the peripheral cytoplasm. Scale bar, 2 μm. (**D**) Examination at high magnification of such cytoplasmic unfenestrated area or FFC (asterisks) show a peculiar structure, with centrally very small fenestrae (small arrow) which form rows of fenestrae with increasing size (large arrow), radiating into the surrounding cytoplasm as a whirlwind. Note the presence of microtubule bundles closely running along the sieve plates (arrowheads). Scale bar, 1 μm. (**E**) Low magnification showing the cell nucleus (N) and the highly fenestrated cytoplasm (small arrow) after 120 minutes of di-h-HALI treatment. Note the thin cytoplasmic arms (arrowheads) which run from the nucleus into the cytoplasm. Inactive FFCs (arrows). Scale bar, 5 μm. (**F**) Higher magnification of the fenestrated cytoplasm shows the presence of FACRs (arrow). From these rings, small interconnecting filaments (arrowheads) seem to cross-link the surrounding cytoskeleton. Scale bar, 250 nm.
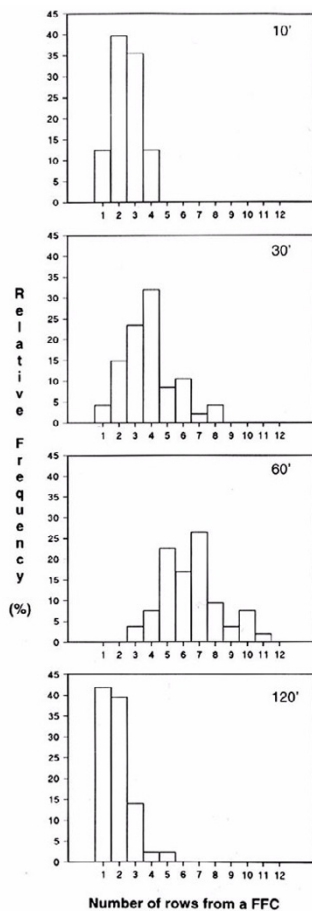
Figure 8
Frequency histogram of the number of fenestrae rows connected to one FFC after 10, 30, 60 and 120 min 100 nM di-h-HALI treatment, extending the static whole-mount TEM images of Figure7. From these histograms it becomes clear that the onset of fenestrae formation starts after 10 min treatment and that the number of fenestrae rows connected to FFCs reaches its maximum at 60 min di-h-HALI treatment. At 120 min of treatment, when the burst of fenestrae formation has subsided (see also, Fig. 7E), a significant shift towards a low number of connected fenestrae rows could be registered.

Figure 9
TEM micrographs of sectioned control- (A-B), and di-h-HALI treated LSECs (C-D).(A) Sectioning through the nuclear region (N) reveals a complex sponge-like appearance of fenestrae lying around the nucleus (arrow). Notice the presence of vacuoles (arrowheads). Scale bar, 1 μm. (**B**) Section through the peripheral cytoplasm reveals fenestrae grouped in sieve plates (large arrow). Note the difference between fenestrae (small arrow), endocytotic vesicles (large arrowhead), and vacuoles (small arrowhead). Scale bar, 1 μm. (**C**) High magnification image of a FFC (large arrow) after 60 minutes of di-h-HALI treatment, showing small fenestrae (small arrowheads), which form rows of fenestrae with increasing size (large arrowheads). Notice filamentous structures (asterisks). Scale bar, 200 nm. (**D**) FFC (large arrow) after 120 minutes of di-h-HALI treatment. Notice the granular pattern of the FFC and the absence of connected fenestrae rows at this stage. Fenestrae (small arrow); filaments (asterisks). Scale bar, 200 nm.

proximately 40% more FFCs per squared micrometer (our unpublished data). While these differences may reflect distinct effects of these two agents on actin; it is possible that they also exert indirect effects on actin binding proteins as is the case with latrunculin [31]. In contrast to the other anti-actin drugs that we tested, the specific alterations that misakinolide and di-h-HALI induce in the state of actin organization either by their barbed end capping activity or by indirect effects on the actin cytoskeleton appear to slow down the process of fenestrae formation to such an extent that it becomes possible to visualize active FFCs. In addition, beside these actin-related effects, possi-
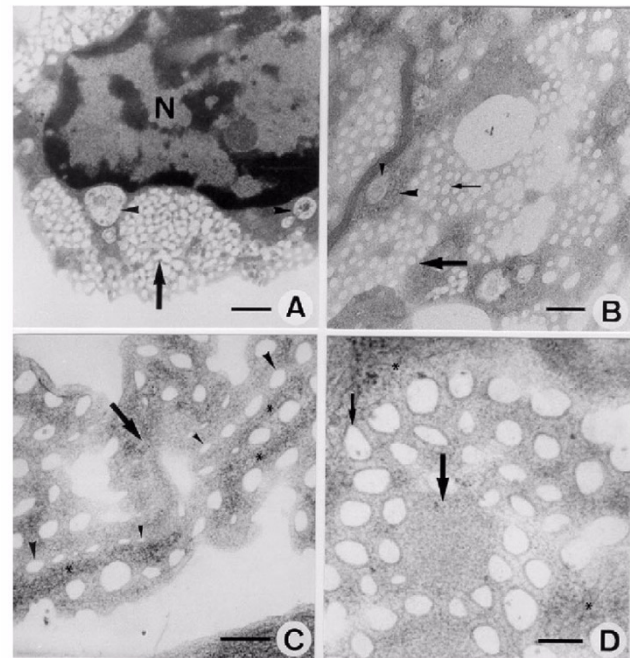
ble membrane-associated interactions of di-h-HALI or misakinolide [23] cannot be excluded and may promote or inhibit the fusion/fission process of the cell membrane during fenestrae formation and as a consequence retard this process in such a way that FFCs appear with connected fenestrae rows. Intrinstingly, it has been recently reported that cytochalasin D facilitates apical membrane invagination and promotes exocytosis in pancreatic acinar cells [32]; whereas cytochalasin B inhibits membrane invagination recovery in neurons [33].

Endothelial cells of large vessels, which normally do not have fenestrae, have the ability to form fenestrae within

minutes [34,35]. This indicates that the process of fenestrae formation probably does not involve de novo synthesis of proteins, but rather a reorganization of preexisting cellular components. Indeed, specialized structures involved in the formation of diaphragmed fenestrae in the capillaries of the exocrine pancreas [36], adrenal cortex [37], kidney glomerulus [38] and tumor micro vascular endothelium [39] have been reported. It is presumed that peristomal rings of cholesterol, knob-like structures, vesiculo-vacuolar organelles and the endothelial pocket may represent important contributors to the formation of diaphragmed fenestrae. Therefore, it is conceivable that fenestrae increase, whether diaphragmed or not, is depending on pre-existing structures which promote fenestrae formation. Although these specialized structures may have an important role in the formation of diaphragmed fenestrae, their role in LSECs is less certain, primarily because LSEC fenestrae lack a diaphragm, are exceptionally abundant, and differ structurally from fenestrae in other blood vessels [1]. The only fenestrae-related structure that LSECs and diaphragmed endothelial cells have in common in the complex process of fenestrae formation is the peristomal ring of sterols surrounding a fenestra [36]. Nonetheless, our observations on the effect of di-h-HALI on large vessel endothelial cells and bone marrow sinusoidal endothelial cells (Fig. 5), demonstrated once more that the increase in the number of fenestrae and the appearance of FFCs by actin-disruption is probably a unique process for the hepatic sinusoidal endothelium. It has been reported that phorbol myristate acetate (PMA) [24] and vascular endothelial growth factor (VEGF) [25,40] could induce diaphraghmed fenestrae in HUVECs. However, De Zanger et al. [41] showed that LSECs are insensible to PMA with regard to fenestrae induction. In addition, Krause and collaborators [42] recently noticed that the increase in the number of fenestrae with time in five days old LSECs cultures is independent of the presence of VEGF. Taking together, these observations clearly illustrate that LSECs respond in a different way to inducers of diaphragmed fenestrae, indicating once more that the machinery for the formation of diaphragmed versus non-diaphragmed fenestrae probably differs. Recent data are accumulating to show that VEGF-induced diaphragmed fenestrae are derived from fused caveolae [39]. A recent study postulates that the same mechanism is used for the formation of LSEC-fenestrae [43,44]. Evidence at the ultrastructural or molecular level about a possible relation between FFCs and interconnected caveolae is absent.

Fusion of two opposing cell membranes to form fenestrae probably requires the presence of unique compositional membrane microdomains and a cell membrane-associated cytoskeletal structure. Several theories have been used to model the possible mechanisms of membrane fusion for LSECs and other cell types. In general, the process leading to membrane fusion and fission is subdivided into different steps, i.e.: adhesion-dehydration; disappearance of the hydration barrier; contact between phospholipid bilayers, and; molecular rearrangement, resulting in pore formation [45,46]. As for LSECs, the first step corresponds to the formation of intramembrane protein-free zones [47], while the appearance of peristomal rings of sterols probably corresponds with the final step [36]. It seems reasonable to assume that these events take place in the rim of FFCs, and that these microdomains contain molecules to pull the bilayers of the cell membranes together at the edge of FFCs. Therefore, to define the FFC more precisely, we applied ultrathin sectioning and showed that filamentous structures of unknown nature are closely associated with these microdomains (Fig. 9C, 9D). In active FFCs, these filaments seem to serve as a guidance for the emerging nascent fenestrae. However, due to technical limitations it is impossible to get a nice plane overview picture of these filamentous structures on EM-sections. These limitations include the extremely small portion of the total cell volume that is included in a section, and the tendency of fine and thin structures cut obliquely or in cross section to disappear visually into the cytoplasmic ground substance. Together, these conditions make it almost impossible to correlate microscopical fluorescence data (Fig. 1B, 1C), with morphologically identified supramolecular structures in TEM (Fig. 9C, 9D). Therefore, in order to clarify the changes in actin organization that underlie the process of fenestrae formation correlative fluorescence- and SEM studies on the same cells was performed (vide infra). Surprisingly, examination of sectioned FFCs did not reveal additional structures regarding the architecture of this singular structure (Fig. 9C, 9D). Detailed investigation showed only a finely granular pattern of intermediate electron density. Although the molecular composition of FFCs remains unknown, F-actin was clearly found to be absent (Fig. 6I, 6L). Steffan et al. [21] postulated based on their in vitro and in situ studies with cytochalasin B that these pore-free microdomains may constitute an anchorage site for cytoskeletal elements. Our TEM sections (Fig. 9C, 9D) and correlative images (Fig. 6) support this statement but show that these cytoskeletal elements do not correspond with filamentous actin. In contrast, these F-actin patches clearly match with the fine globular topographic elevations present on the thin non-fenestrated cytoplasmic arms, and may represent anchor sites for linking F-actin with the plasma membrane [48].

Taking previous [20,21,23,29,47] and present findings together, we propose as an explanation for the events described that FFCs are anchored in the perinuclear area by the actin cytoskeleton where they cannot be resolved by electron microscopy due to their complex multi-fold organization. Disorganization of the filamentous actin cy-

toskeleton results in a centrifugally-like translocation of the FFCs towards the attenuated peripheral cytoplasm. Flattening of the FFCs occurs at the end of this movement and results in the appearance of FFCs with connected rows of fenestrae with increasing diameter. The spiraling rows may indicate that the translocated FFCs are rotating as they move into the peripheral region. The presence of a clear-cut FACR around every single fenestrae indicates that these centers already contain the necessary machinery and/or protein components for assembling the FACR around nascent fenestrae.

However, caution is required when interpreting this hypothesis, because electron microscopy provides only static information. Nevertheless, our data on the number of fenestrae rows connected to one FFC at different time points (Fig. 8), illustrates in one way a dynamic driven process at the level of the FFC. Recent attempts to confirm our hypothesis on the translocation of pre-existing FFC in real-time with atomic force microscopy failed [49,50]. The unique low elastic modulus of living LSECs, together with the damaging tip-sample interactions constitute a problem to acquire sequential images of the process of fenestrae formation in real-time under the influence of cytoskeletal-disturbing agents.

Conclusion
A comparison of all anti-actin agents tested so far, revealed that the only activity that misakinolide and dihydrohalichondramide have in common is their barbed end capping activity; this activity seems to slow down the process of fenestrae formation to such extent that it becomes possible to resolve fenestrae-forming centers; fenestrae formation resulting from microfilament disruption is probably unique to LSECs.

Materials and methods
Cell cultures
The method for the isolation of rat LSECs has been described in detail earlier [51]. Briefly, the liver of a male Wistar rat (Center for Laboratory Animals, Leuven, Belgium – Rats received humane care in compliance with the institution's guidelines for the care and use of laboratory animals in research [accreditation number 99.1-212-3]) was perfused with collagenase A (Boehringer Mannheim, Catalogue Number 1088793, Belgium). After incubation of the fragmented tissue in the same solution, the resulting cell suspension was centrifuged at $100 \times g$ for 5 minutes to remove the parenchymal cells. The supernatant, containing a mixture of sinusoidal liver cells, was then layered on top of a two step Percoll® gradient (25–50%) and centrifuged for 20 minutes at $900 \times g$. The intermediate zone, located between the two density layers was enriched in LSECs. LSEC purity was further enhanced by selective adherence of Kupffer cells and spreading of the LSECs on

collagen. For SEM, LSECs were cultivated in 24-multiwell plates on collagen-coated thermanox cover slips. For whole mount TEM, LSECs were cultivated on collagen-coated nickel grids (300 mesh) instead of cover slips [17]. Formvar (1%) supporting films on nickel grids (300 mesh) were used, coated with diluted collagen (10 μl of collagen-S stock solution [Boehringer Mannheim, Catalogue Number 1098292, Belgium], in 900 μl sterile water). Serum free LSEC culture medium consisted of RPMI-1640 with 2 mM L-glutamine, 100 U/ml penicillin, 100 μg/ml streptomycin and 10 ng/ml endothelial cell growth factor (Boehringer Mannheim, Catalogue Number 1074016, Germany). After 8 hours in culture, LSECs monolayers were extensively washed and subsequently used for experiments. The cultures were estimated to have greater than 95% purity, since less than 5% of the cells examined by EM were devoid of fenestrae.

HUVECs obtained from Clonetics Corporation (BioWhittaker, Catalogue Number CC-0216, New York) were grown to confluency in 24-multiwell plates with or without thermanox cover slips, using endothelial cell growth medium – 2 (BioWhittaker, Catalogue Number CC-3162, New York) supplemented with 2% foetal bovine serum (HyClon Labs, Logan, Utah). The cells were checked routinely for the presence of von Willebrand factor as described earlier [52].

The murine bone marrow sinusoidal endothelial cell line STR-4 (BEC STR-4) was established by transfecting primary endothelial cell cultures with SV40 [53]. BECs STR-4 were maintained in culture in RPMI-1640 supplemented with 2 mM L-glutamine, 100 U/ml penicillin, 100 μg/ml streptomycin, MEM (Gibco Life Sciences, Catalogue Number 11120, Belgium) and 10% bovine serum (fetal Clone I, Hyclone, UT, USA). Cultures were regularly checked for von Willebrand factor positivity and the capacity to uptake LDL [53,54].

Treatment of cells with HALI and di-h-HALI
LSECs and HUVECs were treated with 25, 50, 100 and 200 nM HALI or di-h-HALI for 10, 20, 30, 60 and 120 minutes. The compounds were dissolved in dimethyl sulfoxide (DMSO) and the DMSO concentration in the assays were in all cases ≤ 0.05% and this concentration of DMSO had no effect on the ultrastructure and viability of cells as determined by EM and Hoechst 33342 / propidium iodide staining. Control media also contained DMSO in the same amount as the treated cells. All experimental variables tested, including control cells, were fixed at the same end point, i.e. all cells underwent a two hours treatment with 0.05% DMSO and the compounds were added 10, 20, 30, 60 or 120 minutes prior to fixation [21–23]. After incubation and fixation, cells were prepared for fluorescence microscopy, and EM as described below.

Fluorescence microscopy

In order to visualize simultaneously filamentous (F-actin) and globular (G-actin) actin, LSECs grown on glass cover slips were rinsed twice with phosphate-buffered saline (PBS) at pH 7.4, followed by fixation with freshly prepared 4% formaldehyde in PBS for 15 minutes at 21°C. After fixation, LSECs were submerged in absolute acetone for 3 minutes at -20°C. After this permeabilization, rhodamine-phalloidin (0.165 µM) and fluorescein-DNase I (0.3 µM) solution (Molecular Probes Inc., Eugene-Oregon, USA) was applied to LSECs for 20 minutes at 21°C. LSECs were subsequently washed 10 × with PBS and mounted on microscope slides in Vectashield containing DAPI (Vector Laboratories Inc., Burlingame, USA). As a control for the specificity of the staining reactions, LSECs were incubated first with 0.165 µM unlabeled phalloidin (Molecular Probes Inc., P-3457, Eugene-Oregon, USA) and 0.3 µM DNase I (Boehringer Mannheim S.A., Catalogue Number 104132, Germany) solution for 20 minutes at 21°C, before incubation with rhodamine-phalloidin and fluorescein-DNase I. No F- or G-actin staining was observed when control LSECs were incubated with unlabeled phalloidin or DNase I.

Cells were viewed and recorded with a Leica DM-IRBE inverted microscope, equipped with a Leica WILD MPS 48/52 – 35 mm camera. Elite Chrome 400 ASA slide film was used and slides were digitally scanned using a Minolta Dimâge Multi Scanner. The obtained images were transferred to Adobe Photoshop 5.5 software for color channel analysis and figure assembly. The magnification of the microscope was calibrated using fluoresbrite™ calibration grade microspheres, (Polylab BVBA, Ø 3.0 µm, Catalogue Number 18861, Belgium).

Scanning electron microscopy

Cells were rinsed twice with PBS and fixed with 2% glutaraldehyde in Na-cacodylate buffer (0.1 M and 0.1 M sucrose) at pH 7.4 for 12 hours. They were subsequently treated with filtered 1% tannic acid in 0.15 M Na-cacodylate at pH 7.4 for 1 hour and postfixed with 1% osmium tetroxide in 0.1 M Na-cacodylate at pH 7.4 for 1 hour. SEM samples were dehydrated in a graded ethanol series, dried with hexamethyldisilazane, and sputter coated with 10 nm of gold. The samples were examined with a Philips SEM 505 (Philips Eindhoven, The Netherlands) at an accelerating voltage of 30 KV [55].

For automatic image analysis, the SEM was regularly calibrated at a magnification of × 20,000, using a 28.800 lines/inch grating stub with the specimen in eucentric position. 30 images at a magnification of × 20,000 were taken in randomly selected fields of each experimental variable, each image containing a minimum of 10 fenestrae. Digital images with a low-noise content were ob-

tained by using a large spot size (20 nm) and were processed subsequently and stored on a Masscomp 5520S computer, running under the RTU UNIX operating system, as previously described [51].

Correlative fluorescence- and scanning electron microscopy

Cells cultured on collagen-coated CELLocate-microgrid® glass cover slips (Eppendorf, Catalogue Number 5245 962.004-00, Hamburg, Germany) were treated with HALI or di-h-HALI as described and subsequently stained with rhodamine-phalloidin to visualize F-actin by fluorescence microscopy (see "Fluorescence microscopy" section). Photographs were then taken with the fluorescence microscope and photographed cells were located simultaneously by using the alphanumerically marked grids on the cover slip. Cover slips were recovered and transferred to 2% glutaraldehyde in Na-cacodylate buffer for 12 hours and further processed for scanning electron microscopy [55]. Previously visualized cells in the fluorescence microscope were relocated with the aid of the alphanumerically marks on top of the cover slips and SEM-images of the corresponding cells were taken. Images of the same cells obtained from both microscopies were printed at an identical photographic end magnification [56], and were digitized using a Hewlett Packard ScanJet 3c scanner. The obtained images were transferred to Adobe Photoshop 5.5 software for color adjustment and figure assembly by using the replace color and duplicate layer/merge options.

Transmission electron microscopy

In order to visualize the cytoskeleton as a whole-mount for TEM [17], cells cultured on collagen-coated nickel grids were rinsed twice with PBS and slightly fixed for 1 minute with freshly prepared 4% formaldehyde in PBS at 21°C. Cells were subsequently extracted in cytoskeleton buffer consisting of 1 mM ethylene glycol bis [2-aminoethylether]-N,N,N',N' tetra-acetic acid, 100 mM piperazine-N,N'-bis [2-ethanesulfonic acid], 4% polyethylene glycol 6000 and 0.1% Triton X-100 in PBS at pH 6.9 for 1 minute at 21°C. After extraction, cells were processed as for SEM, but the tannin was omitted. Samples were further dehydrated and hexamethyldisilazane-dried. The specimens were examined in a Philips Tecnai 10 (Philips Eindhoven, The Netherlands) at an accelerating voltage of 100 kV.

For sectioning, cells cultured on cover slips were fixed and dehydrated in the same way as for SEM. After dehydration, samples were embedded in Epon and after hardening of the embedding medium, the cover slips were removed using liquid nitrogen. Sections of 60 nm under various angles were cut with a diamond knife, stained first with uranyl acetate, subsequently with lead citrate, and examined in a Philips Tecnai 10 at 80 kV as described [51].

Statistical analysis

All experiments were repeated five times. Statistical analysis was performed with the Mann-Whitney U test.

List of abbreviations used

LSECs, liver sinusoidal endothelial cells; FACR, fenestrae-associated cytoskeleton ring; FFCs, fenestrae-forming centers; HALI, halichondramide; di-h-HALI dihydrohalichondramide; HUVECs, human umbilical vein endothelial cells; BECs STR-4, bone marrow sinusoidal endothelial cells STR-4; F-actin, filamentous actin; G-actin, globular actin; PBS, phosphate-buffered saline.

Acknowledgements

References

1. Wisse E: **An electron microscopic study of the fenestrated endothelial lining of rat liver sinusoids.** *J Ultrastruct Res* 1970, **31**:125-150
2. Wisse E, De Zanger RB, Charels K, Van Der Smissen P, McCuskey RS: **The liver sieve: Considerations concerning the structure and function of endothelial fenestrae, the sinusoidal wall and the space of Disse.** *Hepatology* 1985, **5**:683-692
3. Popescu D, Movileanu L, Ion S, Flonta ML: **Hydrodynamic effects on the solute transport across endothelial pores and hepatocyte membranes.** *Phys Med Biol* 2000, **45**:N157-N165
4. Fraser R, Dobbs BR, Rogers GWT: **Lipoproteins and the liver sieve: the role of the fenestrated sinusoidal endothelium in lipoprotein metabolism, atherosclerosis, and cirrhosis.** *Hepatology* 1995, **21**:863-874
5. Braet F, Luo D, Spector I, Vermijlen D, Wisse E: **Endothelial and pit cells.** *In: The liver: Biology and Pathobiology* 2001, 437-453
6. Wack KE, Ross MA, Zegarra V, Sysko LR, Watkins SC, Stolz DB: **Sinusoidal ultrastructure evaluated during the revascularization of regenerating rat liver.** *Hepatology* 2001, **33**:363-378
7. Sato Y, Tsukada K, Hatakeyama K: **Role of shear stress and immune responses in liver regeneration after a partial hepatectomy.** *Surg Today* 1999, **29**:1-9
8. Romero EL, Morilla MJ, Regts J, Koning GA, Scherphof GL: **On the mechanism of hepatic transendothelial passage of large liposomes.** *FEBS Lett* 1999, **448**:193-196
9. Le Bail B, Bioulac-Sage P, Senuita R, Quinton A, Saric J, Balabaud C: **Fine structure of hepatic sinusoids and sinusoidal cells in disease.** *J Electron Micr Tech* 1990, **14**:257-282
10. Deaciuc IV, D'Souza NB, Sarphie TG, Schmidt J, Hill DB, McClain CJ: **Effects of exogenous superoxide anion and nitric oxide on the scavenging function and electron microscopic appearance of the sinusoidal endothelium in the isolated, perfused rat liver.** *J Hepatol* 1999, **30**:213-221
11. Takashimizu S, Watanabe N, Nishizaki Y, Kawazoe K, Matsuzaki S: **Mechanisms of hepatic microcirculatory disturbances induced by acute ethanol administration in rats, with special reference to alterations of sinusoidal endothelial fenestrae.** *Alcohol Clin Exp* 1999, **23**:39S-46S
12. Clark SA, Angus HB, Cook HB, Oxner RBG, George PM, Fraser R: **Defenestration of hepatic sinusoids as a cause of hyperlipoproteinaemia in alcoholics.** *Lancet* 1988, **2**:1225-1227
13. Arias IM: **The biology of hepatic endothelial cell fenestrae. In:** *Progress in Liver Diseases IX* 1990, 11-26
14. Brauneis U, Gatmaitan Z, Arias IM: **Serotonin stimulates a Ca²⁺ permeant nonspecificcation channel in hepatic endothelial cells.** *Biochem Biophys Res Commun* 1992, **186**:1560-1566
15. Gatmaitan Z, Varticovski L, Ling L, Mikkelsen R, Steffan AM, Arias IM: **Studies on fenestral contraction in rat liver endothelial cells in culture.** *Am J Pathol* 1996, **148**:2027-2041
16. Yokomori H, Oda M, Kamegaya Y, Tsukada N, Nakamura M, Ishii H: **Hepatic sinusoidal endothelial fenestrae express plasma membrane Ca⁺⁺ pump and Ca⁺⁺Mg⁺⁺-ATPase.** *Liver* 2000, **20**:458-464
17. Braet F, De Zanger R, Baekeland M, Crabbé E, Van Der Smissen P, Wisse E: **Structure and dynamics of the fenestrae-associated cytoskeleton of rat liver sinusoidal endothelial cells.** *Hepatology* 1995, **21**:180-189
18. Nishimura Y, Lemasters JL: **Mitochondrial dysfunction and cytoskeletal disruption during hypoxia to cultured rat hepatic sinusoidal endothelial cells: the pH paradox and cytoprotection by glucose, acidotic pH, and glycine.** *Hepatology* 1998, **27**:1039-1049
19. Upadhya GA, Strasberg SM: **Evidence that actin disassembly is a requirement for matrix metalloproteinase secretion by sinusoidal endothelial cells during cold preservation in the rat.** *Hepatology* 1999, **30**:169-176
20. Spector I, Braet F, Shochet NR, Bubb MR: **New anti-actin drugs in the study of the organization and function of the actin cytoskeleton.** *Micr Res Techn* 1999, **47**:18-37
21. Steffan AM, Gendrault JL, Kirn A: **Increase in the number of fenestrae in mouse endothelial liver cells by altering the cytoskeleton with cytochalasin B.** *Hepatology* 1987, **7**:1230-1238
22. Braet F, De Zanger R, Jans D, Spector I, Wisse E: **Microfilament-disrupting agent latrunculin A induces an increased number of fenestrae in rat liver sinusoidal endothelial cells: comparison with cytochalasin B.** *Hepatology* 1996, **24**:627-635
23. Braet F, Spector I, De Zanger R, Wisse E: **A novel structure involved in the formation of liver endothelial cell fenestrae revealed by using the actin inhibitor misakinolide.** *Proc Natl Acad Sci USA* 1998, **95**:13635-13640
24. Lombardi T, Montesano R, Orci L: **Phorbol ester induces diaphragmed fenestrae in large vessel endothelium in vitro.** *Eur J Cell Biol* 1987, **44**:86-89
25. Esser S, Wolburg K, Wolburg H, Breier G, Kurzchalia T, Risau W: **Vascular endothelial growth factor induces endothelial fenestration in vitro.** *J Cell Biol* 1998, **140**:947-959
26. Soda R, Tavassoli M: **Mapping of the bone marrow sinus endothelium with lectins and glycosylated ferritins: identification of differentiated microdomains and their functional significance.** *J Ultrastruct Res* 1983, **84**:299-310
27. Inoue S, Osmond DG: **Basement membrane of mouse bone marrow sinusoids shows distinctive structure and proteoglycan composition: a high resolution ultrastructural study.** *Anat Rec* 2001, **264**:294-304
28. Lindroth M, Bell PB, Fredriksson BA, Xiao-Dong L: **Preservation and visualisation of molecular structure in detergent-extracted whole mounts of cultured cells.** *Micr Res Techn* 1992, **22**:130-150
29. Taira K: **Trabecular meshworks in the sinusoidal endothelial cells of the golden hamster: a freeze-fracture study.** *J Submicrosc Cytol Pathol* 1994, **26**:271-277
30. Bubb MR, Spector I: **Use of the F-actin binding drugs misakinolide A and swinholide A.** *Methods Enzymol* 1998, **298**:26-32
31. Yarmola EG, Somasundaram T, Boring TA, Spector I, Bubb MR: **Actin-latrunculin A structure and function: Differential modulation of actin-binding protein function by latrunculin A.** *J Biol Chem* 2000, **275**:28120-28127
32. Valentijn KM, Gumkowski FD, Jamieson JD: **The subapical actin cytoskeleton regulates secretion and membrane retrieval in pancreatic acinar cells.** *J Cell Sci* 1999, **112**:81-96
33. Herring TL, Cohan CS, Welnhofer EA, Mills LR, Morris CE: **F-actin at newly invaginated membrane in neurons: implications for surface area regulation.** *J Membr* 1999, **171**:151-169

34. Roberts WG, Palade GE: **Increased microvascular permeability and endothelial fenestration induced by vascular endothelial growth factor.** *J Cell Sci* 1995, **108:**2369-2379

35. Predescu D, Ihida K, Predescu S, Palade GE: **The vascular distribution of the platelet-activating factor receptor.** *Eur J Cell Biol* 1996, **69:**86-98

36. Simionescu N, Lupu F, Simionescu M: **Rings of membrane sterols surround the openings of vesicles and fenestrae, in capillary endothelium.** *J Cell Biol* 1983, **97:**1592-1600

37. Milici AJ, Furie MB, Carley WW: **The formation of fenestrations and channels by capillary endothelium in vitro.** *Proc Natl Acad Sci USA* 1985, **82:**6181-6185

38. Milici AJ, Peters KR, Palade GE: **The endothelial pocket. A new structure in fenestrated endothelia.** *Cell Tissue Res* 1986, **244:**493-499

39. Feng D, Nagy JA, Pyne K, Hammel I, Dvorak HF, Dvorak AM: **Pathways of macromolecular extravasation across microvascular endothelium in response to VPF/VEGF and other vasoactive mediators.** *Microcirculation* 1999, **6:**23-44

40. Chen J, Braet F, Brodsky S, Weinstein T, Romanov V, Noiri E, Goligorsky MS: **VEGF-induced mobilization of caveolae and increase in permeability of endothelial cells.** *Am J Physiol Cell Physiol* 2002, **282:**C1053-1063

41. De Zanger R, Braet F, Arnez Camacho MR, Wisse E: **Prolongation of hepatic endothelial cell cultures by phorbol myristate acetate.** *In: Cells of the Hepatic Sinusoid* 1997, 97-101

42. Krause P, Markus PM, Schwartz P, Unthan-Fechner K, Pestel S, Fandrey J, Probst I: **Hepatocyte-supported serum-free culture of rat liver sinusoidal endothelial cells.** *J Hepatol* 2000, **32:**718-726

43. Oda M, Yokomori H, Han J, Kamegaya Y, Ogi M, Nakamura M: **Hepatic sinusoidal endothelial fenestrae are a stationary type of fused and interconnected caveolae.** *In: Cells of the Hepatic Sinusoid* 2001, 94-98

44. Yokomori H, Oda M, Ogi M, Kamegaya Y, Tsukada N, Ishii H: **Endothelial nitric oxide synthase and caveolin-1 are co-localized in sinusoidal endothelial fenestrae.** *Liver* 2001, **21:**198-206

45. Lindau M, Almers W: **Structure and function of fusion pores in exocytosis and exoplasmic membrane fusion.** *Curr Opin Cell Biol* 1995, **7:**509-517

46. Monck JR, Fernandez JM: **The fusion pore and mechanisms of biological membrane fusion.** *Curr Opin Cell Biol* 1996, **8:**524-533

47. Bingen A, Gendrault JL, Kirn A: **Cryofracture study of fenestrae formation in mouse liver endothelial cells treated with cytochalasin B.** *In: Cells of the Hepatic Sinusoid* 1989, 466-470

48. Bershadsky AD, Glück U, Denisenko ON, Sklyarova TV, Spector I, Ben-Ze'ev A: **The state of actin assembly regulates actin and vinculin expression by a feedback loop.** *J Cell Sci* 1995, **108:**1183-1193

49. Braet F, Rotsch C, Wisse E, Radmacher M: **Comparison of fixed and living liver endothelial cells by atomic force microscopy.** *Appl Phys A* 1998, **66:**S575-S578

50. Braet F, De Zanger R, Seynaeve C, Baekeland M, Wisse E: **A comparative atomic force microscopy study on living skin fibroblasts and liver endothelial cells.** *J Electron Microsc* 2001, **50:**283-290

51. Braet F, De Zanger R, Sasaoki T, Baekeland M, Janssens P, Smedsrød B, Wisse E: **Assessment of a method of isolation, purification and cultivation of rat liver sinusoidal endothelial cells.** *Lab Invest* 1994, **70:**944-952

52. Jaffe EA, Nachman RL, Becker CG, Minick CR: **Culture of human endothelial cells derived from umbilical veins. Identification by morphologic and immunologic criteria.** *J Clin Invest* 1973, **52:**2745-2756

53. Imai K, Kobayashi M, Wang J, Ohiro Y, Hamada J, Cho Y, Imamura M, Musashi M, Kondo T, Hosokawa M, Asaka M: **Selective transendothelial migration of hematopoietic progenitor cells: a role in homing of progenitor cells.** *Blood* 1999, **93:**149-156

54. Vanderkerken K, De Greef C, Asosingh K, Arteta B, De Veerman M, Vandebroek I, Van Riet I, Kobayashi M, Smedrød B, Van Camp B: **Selective initial in vivo homing pattern of 5T2 multiple myeloma cells in the C57BlKaLwRij mouse.** *Br J Cancer* 2000, **82:**953-959

55. Braet F, De Zanger R, Wisse E: **Drying cells for SEM, AFM and TEM by hexamethyldisilazane: a study on hepatic endothelial cells.** *J Microsc* 1997, **186:**84-87

56. Mironov AA, Polishchuk RS, Luini A: **Visualizing membrane traffic in vivo by combined video fluorescence and 3D electron microscopy.** *Trends Cell Biol* 2000, **10:**349-353